INVESTIGATED BEHAVIOR OF THE TOP-BASE FOUNDATION USING FINITE ELEMENT ANALYSIS

My PHAM*, Khanh-Toan LE

The University of Danang - University of Science and Technology

*Corresponding author: pmy@dut.udn.vn

(Received: April 24, 2022; Accepted: June 9, 2022)

Abstract - Top-base foundation (TBF) is a cutting-edge technology in construction area. It is in terms of increasing the load-carrying capacity of the ground, reducing settlement, especially the difference in settlement between the footings, resisting earthquake loads, fast construction, friendly environment, and low construction cost. To date, most of the research has mainly focused on field and laboratory experimental studies. These studies require large costs, and take a long time. In addition, most practical experiments only determine the displacement field, while the stress field is difficult to determine precisely. Therefore, in this study, a finite element analysis (FEA) is proposed based on verification with the experimental results of previous studies. Consequently, the accuracy and reliability of the FEA can be assessed. Through the FEA procedure, it is possible to predict the stress field with high reliability, which can be applied in practice, bringing economic efficiency, especially suitable for current conditions in Vietnam.

Key words - Top-block; Top-base foundation (TBF); Settlement; Bearing capacity; Finite element analysis

1. Introduction

TBF technology originated in Japan in the early 1980s. After the great earthquakes in Chiba in 1987 and Kobe in 1995, the buildings designed with TBFs were virtually undamaged. Many theoretical and experimental studies have been conducted to explain the effectiveness of the TBF and have been published in Japanese geotechnical journals as well as at international conferences on foundation treatment methods [1-4]. In the early 1990s, TBF technology was studied and applied in Korea and there have been important improvements in the field of construction. In Korea, top-blocks are cast in situ concrete using recycled plastic molds, which are very eco-friendly [5-7]. TBF technology in Korea is not manufactured at the factory. Hence, there is no need for a warehouse to store the top blocks. This technology also prevents the cracks from occurring during transportation, from the factory to the construction site, or during loading and unloading of top-blocks, or during top-block installation process. It also simultaneously limits the crane shift during production, transportation as well as construction [8]. The result is to improve construction efficiency, shorten construction schedule, and reduce construction costs.

The bearing capacity studies of the TBF by field tests through the plate load test method have demonstrated that the bearing capacity of the TBF increases from 50% to 100%, and the ability to restrict settlement decreases from 30% to 50% compared to the original soil ground when not treated with top-base technology [3, 5, 7, 9]. In 2010, Kim et. al, conducted a re-evaluation of the bearing capacity and settlement limitation of the TBF in the laboratory with a scaled model of 1/5 compared to the actual model at the construction site [10]. The results were performed on 100 test samples and the author concluded that the bearing capacity and settlement limitation of the TBF between the field test and the laboratory test were appropriate.

Other studies use analytical and numerical methods to comprehend the working mechanism of the TBF for the effect of significantly reducing the load transfer from the foundation to the ground, limiting the settlement of the soil ground, and force distribution mechanism between top blocks and crusher-run [8, 11]. These studies do not verify or evaluate the accuracy and reliability of the numerical model for field tests. Therefore, in this study the FEA is used with improved theories and algorithms to enhance the efficiency of the numerical model. Then, it is verified with the actual model to evaluate the accuracy and reliability of the numerical model. If the evaluation results are reliable, the numerical model can be exerted instead of the field tests to resolve the cost and implementation time of the projects.

2. Finite element analysis of top-base foundation

2.1. The governing equation description of TBF ground

TBF ground is considered as a porosity material. Behavior of TBF ground involves the fluid inside porous space and soil skeleton. In this study, the stresses of an isotropic porous elastic material containing fluid is exerted to describe stress state in TBF ground. According to Terzaghi's principle [12, p.84], the stress in TBF ground is described as follows [13]:

$$\boldsymbol{\sigma} = \boldsymbol{\sigma}' + \mathbf{m}\ p_{steady} + p_{\text{excess}} \tag{1}$$

In which $\boldsymbol{\sigma}' = \begin{bmatrix} \sigma'_{xx} & \sigma'_{yy} & \sigma'_{zz} & \sigma'_{xy} & \sigma'_{yz} & \sigma'_{zx} \end{bmatrix}^T$ is identified as the effective stress. It is only generated by soil skeleton that neglected the stresses due to fluid; Because fluid in porous space only exists spherical stress (no deviatoric stress), as a result vector $\mathbf{m} = \begin{bmatrix} 1 & 1 & 1 & 0 & 0 & 0 \end{bmatrix}^T$, p_{steady} is caused by groundwater level; p_{excess} is due to the excess pore pressure.

The correlation between stress state σ and body force $\mathbf{b}$ is described in the static equilibrium of a continuum deformation. Its strong form(1a) can be formulated as [14, 15]:

$$\mathbf{L}^T\boldsymbol{\sigma} + \mathbf{b} = 0 \tag{2}$$

where $\mathbf{L}^T$ is the transpose(2a) of a differential operator, defined as:

$$\mathbf{L}^T = \begin{bmatrix} \frac{\partial}{\partial x} & 0 & 0 & \frac{\partial}{\partial y} & 0 & \frac{\partial}{\partial z} \\ 0 & \frac{\partial}{\partial y} & 0 & \frac{\partial}{\partial x} & \frac{\partial}{\partial z} & 0 \\ 0 & 0 & \frac{\partial}{\partial z} & 0 & \frac{\partial}{\partial y} & \frac{\partial}{\partial x} \end{bmatrix} \quad (3)$$

Most FEA problems are described under the integral form. The goal is to easily impose boundary conditions and solve problems on the whole mechanical system. Using Galerkin's variation principle, the governing Eq. (2) is reformulated under the integral form as bellows:

$$\int \delta\mathbf{u}^T \ \mathbf{L}^T\boldsymbol{\sigma} + \mathbf{b}\, dV = 0 \quad (4)$$

In which $\delta\mathbf{u}$ represents a kinematically admissible variation of displacements; $\mathbf{t}$ represents the tractions on surface S; $\boldsymbol{\varepsilon}$ is the strain state(3a) related to the stress state under rate form e.g., $\dot{\boldsymbol{\sigma}} = \mathrm{M}\dot{\varepsilon}$. Green's theorem is employed to expand the partial integration with respect to the first term of Eq. (4). The result leads to(4a):

$$\int \delta\varepsilon^T\boldsymbol{\sigma} dV = \int \delta\mathbf{u}^T\mathbf{b} dV + \int \delta\mathbf{u}^T\mathbf{t} dV \quad (5)$$

An incremental process with respect to stress such as $\boldsymbol{\sigma}^i = \boldsymbol{\sigma}^{i-1} + \Delta\boldsymbol{\sigma}$ with $\Delta\boldsymbol{\sigma} = \int \dot{\boldsymbol{\sigma}} dt$ to assess the development of stress state in entire structure. As a result, the Eq. (5)(5a) can be rewritten as bellows:

$$\int \delta\varepsilon^T \Delta\boldsymbol{\sigma} dV = \int \delta\mathbf{u}^T\mathbf{b}^i dV + \int \delta\mathbf{u}^T\mathbf{t}^i dS - \int \delta\varepsilon^T\boldsymbol{\sigma}^{i-1} dV \quad (6)$$

2.2. Continuity equation of underground water flow motion

TBF ground is assumed as an isotropic porous medium, due to the mass conservation, it means the water outflow from volume is equal to the changes in the mass concentration [16, 17].

$$\boldsymbol{\nabla}^T \left\{ \frac{k_{rel}}{\rho_{\mathrm{w}} g} \mathbf{k}^{sat} \boldsymbol{\rho}_{\mathrm{w}} \ \boldsymbol{\nabla} p_{\mathrm{w}} + \rho_{\mathrm{w}} g \right\} = -\frac{\partial}{\partial t} \ \boldsymbol{\rho}_{\mathrm{w}} n S \quad (7)$$

In which n, S, g, ρ_{w}, p_{w} and k_{rel} are the porosity, the degree of saturation of the soil, the acceleration vector due to gravity, the density of water, the water pore pressure and the ratio of permeability at a given saturation to the permeability in saturation state $\mathbf{k}^{sat}$ respectively.

$$\mathbf{k}^{sat} = \begin{bmatrix} k_x^{sat} & 0 & 0 \\ 0 & k_y^{sat} & 0 \\ 0 & 0 & k_z^{sat} \end{bmatrix} \quad (8)$$

Set $\mathbf{q} = \left\{ \frac{k_{rel}}{\rho_{\mathrm{w}} g} \mathbf{k}^{sat} \ \boldsymbol{\nabla} p_{\mathrm{w}} + \rho_{\mathrm{w}} g \right\}$ $**$, it is identified as the specific discharge. In addition, the deformation of soil skeleton partials and the gradients of the density of water (according to Boussinesq's approximation) are neglected. Hence the equation can be rewritten under simple form as:

$$\boldsymbol{\nabla}^T \cdot \ \boldsymbol{\rho}_{\mathrm{w}}\mathbf{q} \ + S\mathbf{m}^T \frac{\partial\boldsymbol{\varepsilon}}{\partial t} - n\left(\frac{S}{K_{\mathrm{w}}} - \frac{\partial S}{\partial p_{\mathrm{w}}}\right)\frac{\partial p_{\mathrm{w}}}{\partial t} = 0 \quad (9)$$

Where K_{w} is the bulk modulus of the pore fluid.

2.3. Finite element discretization

The TBF is discrete into a number of elements. Each element consists of number of degrees of freedom that correspond to the displacement/pore-pressure components. It generates a displacement/pore-pressure field of element that is obtained from the discrete nodal values $\boldsymbol{v}$ and $\mathbf{p}_n$ as shown in Eq. (10). Where matrix $\mathbf{N}$ is arranged from shape functions (interpolation functions).

$$\mathbf{u} = \mathbf{N}\boldsymbol{v} \quad and \quad \mathbf{p} = \mathbf{N}\mathbf{p}_n \quad (10)$$

Element deformation correlated to its displacement field through the kinematic relation e.g., $\varepsilon = \mathbf{L}\mathbf{u}$ $*$. Substituting(6a) $\mathbf{u}$ in Eq. (10) into relationship $*$ leads to:

$$\varepsilon = \mathbf{L}\mathbf{N}\boldsymbol{v} = \mathbf{B}\boldsymbol{v} \quad (11)$$

Note that the relationship in Eq. (10) and Eq. (11) can be exerted in every rate, incremental, variational form. Therefore, they can be substituted into Eq. (6) so that it may be reformulated under following incremental form:

$$\int \mathbf{B}^T \Delta\boldsymbol{\sigma} dV = \int \mathbf{N}^T \Delta\mathbf{b} dV + \int \mathbf{N}^T \Delta\mathbf{t} dS + \mathbf{R}_0 \quad (12)$$

with $\mathbf{R}_0 = \int \mathbf{N}^T\mathbf{b}_0 dV + \int \mathbf{N}^T\mathbf{t}_0 dS - \int \mathbf{B}^T\boldsymbol{\sigma}_0 dV$

The constitutive equation is presented under the nodal equilibrium relationship by dividing the total stresses into pore pressure and effective stresses according to Eq. (1) as following equation:

$$\mathbf{K}\Delta\boldsymbol{v} + \mathbf{L}\Delta\mathbf{p}_n = \Delta\mathbf{f}_n \quad (13)$$

where $\mathbf{K}$, $\mathbf{L}$ and $\mathbf{f}$ are the stiffness matrix, the coupling matrix, and the incremental load vector. They are given as follows:

$$\begin{cases} \mathbf{K} = \int \mathbf{B}^T\mathbf{M}\mathbf{B} dV \\ \mathbf{L} = \int \mathbf{B}^T\mathbf{m}\mathbf{N} dV \\ \Delta\mathbf{f}_n = \int \mathbf{N}^T\Delta\mathbf{b} dV + \int \mathbf{N}^T\Delta\mathbf{t} dS \end{cases} \quad (14)$$

For the underground water flow motion, the $\rho_{\mathrm{w}}\mathbf{q}$ is adopted as bellows:

$$\boldsymbol{\rho}_{\mathrm{w}}\mathbf{q} = \mathbf{k}\nabla\left(\frac{\gamma_{\mathrm{w}} y - p_{steady} - p}{\gamma_{\mathrm{w}}}\right) \quad (15)$$

where γ_{w} is the unit weight of the pore fluid, $\mathbf{k} = k_{rel}\mathbf{k}^{sat}$, and $\mathbf{k}$ is defined as:

$$\mathbf{k} = \begin{bmatrix} k_x & 0 & 0 \\ 0 & k_y & 0 \\ 0 & 0 & k_z \end{bmatrix} \quad (16)$$

A Galerkin procedure is employed for finite element discretization, and simultaneously prescribed boundary conditions with respect to Eq. (9) and Eq. (15) as given:

$$\mathbf{L}^T\frac{\partial v}{\partial t} - \mathbf{H}\mathbf{p}_n - \mathbf{S}^T\frac{\partial\mathbf{p}_n}{\partial t} = \mathbf{q}_n \quad (17)$$

where $\mathbf{q}_n$ is determined as in formula $**$, it is a vector due to the prescribed outflow at the boundary; $\mathbf{H}$ and $\mathbf{S}$ are given as follows:

$$\begin{cases} \mathbf{S} = \int \dfrac{n}{K_w} \mathbf{N}^T \mathbf{N} dV \\ \mathbf{H} = \int \nabla \cdot \mathbf{N}^T \mathbf{k} \nabla \cdot \mathbf{N} \, dV \end{cases} \quad (18)$$

Applying the incremental algorithm and integration procedure to solve the Eq. (17). Its form is given as bellows:

$$\mathbf{L}^T \Delta \boldsymbol{v} - \Delta t \mathbf{H}^* \mathbf{p}_{n0} - \mathbf{S}^* \Delta \mathbf{p}_n = \Delta t \mathbf{q}_n \quad (19)$$

where $\mathbf{S} = \alpha \Delta t \mathbf{H} + \mathbf{S}$, $\mathbf{q}_n^* = \mathbf{q}_{n0} + \alpha \Delta \mathbf{q}_n$, the parameter α is the time integration coefficient, subscript indicator 0 denotes value at the beginning of a time step.

Finally, a compact form of finite element analysis, it is cooperated between Eq. (13) and Eq. (19) with respect to TBF ground gives:

$$\begin{bmatrix} \mathbf{K} & \mathbf{L} \\ \mathbf{L}^T & -\mathbf{S}^* \end{bmatrix} \begin{bmatrix} \Delta \boldsymbol{v} \\ \Delta \mathbf{p}_n \end{bmatrix} = \begin{bmatrix} 0 & 0 \\ 0 & \Delta t \mathbf{H}^* \end{bmatrix} \begin{bmatrix} \boldsymbol{v}_0 \\ \mathbf{p}_{n0} \end{bmatrix} + \begin{bmatrix} \Delta \mathbf{f}_n \\ \Delta t \mathbf{q}_n \end{bmatrix} \quad (20)$$

2.4. Interaction between top blocks and TBF ground

In this study, FEA of top block is not(7a) presented because it is the special case of TBF ground when the porosity effect is neglected. The interface between top block and TBF ground is described by an embedded element. The top block force vector $\mathbf{t}^{TB}$ characterized for the interaction between top block and its ground. Using incremental algorithm, the development of the $\mathbf{t}_0^{TB}$ at initial time (it's so-called initial force) after each force increment $\Delta \mathbf{t}^{TB}$ is presented as bellows:

$$\mathbf{t}^{TB} = \mathbf{t}_0^{TB} + \Delta \mathbf{t}^{TB} \quad (21)$$

The institutive equation between the interface traction increment and the relative displacement increment is formulated as:

$$\Delta \mathbf{t}^{TB} = \mathbf{D}^{TB} \Delta \mathbf{u}_{rel} \quad (22)$$

Applied the virtual work into Eq. (22), it can be written as:

$$\delta u_{rel}^T \Delta t^{TB} = \delta v_{rel}^T \mathbf{N}_{rel}^T \mathbf{D}^{TB} \mathbf{N}_{rel} \Delta \boldsymbol{v}_{rel} = \mathbf{K}^{TB} \Delta \boldsymbol{v}_{rel} \quad (23)$$

In which $\mathbf{K}^{TB}$ is the stiffness matrix at top block interface and it is given as:

$$\mathbf{K}^{TB} = \begin{bmatrix} \mathbf{K}_{bb}^{TB} & \mathbf{K}_{bs}^{TB} \\ \mathbf{K}_{sb}^{TB} & \mathbf{K}_{ss}^{TB} \end{bmatrix} \quad (24)$$

here

$$\begin{cases} \mathbf{K}_{bb}^{TB} = \mathbf{N}_b^T \mathbf{D}^{TB} \mathbf{N}_b & : \text{contribution of the top block nodes} \\ \mathbf{K}_{ss}^{TB} = \mathbf{N}_s^T \mathbf{D}^{TB} \mathbf{N}_s & : \text{contribution of the soil nodes} \\ \mathbf{K}_{bs}^{TB} = -\mathbf{N}_b^T \mathbf{D}^{TB} \mathbf{N}_s & : \text{mixed top-block and soil nodes} \\ \mathbf{K}_{bs}^{TB} = -\mathbf{N}_b^T \mathbf{D}^{TB} \mathbf{N}_s & : \text{mixed soil and top-block nodes} \end{cases} \quad (25)$$

2.5. Material model for top base foundation ground

This study uses Mohr-Coulomb model. Consequently, the strain is separated into elastic and plastic strains [18]. It is given in the rate form as:

$$\dot{\boldsymbol{\varepsilon}} = \dot{\boldsymbol{\varepsilon}}^e + \dot{\boldsymbol{\varepsilon}}^p \quad (26)$$

The constitutive relation between effective stress and elastic strain is formulated under following rate form in which $\mathbf{D}$ is incremental elastic stress-train matrix:

$$\dot{\boldsymbol{\sigma}}' = \mathbf{D} \dot{\boldsymbol{\varepsilon}}^e = \mathbf{D} \left(\boldsymbol{\varepsilon} - \dot{\boldsymbol{\varepsilon}}^p \right) \quad (27)$$

The plastic train increment $\dot{\varepsilon}^p$ is formulated as:

– The case of associated plasticity

$$\dot{\boldsymbol{\varepsilon}}^P = \lambda \frac{\partial f}{\partial \dot{\boldsymbol{\sigma}}} \quad \text{with} \quad f = \frac{1}{2} \left(\sigma_3 - \sigma_1 \right) + \frac{1}{2} \left(\sigma_3 + \sigma_1 \right) \sin\varphi - c\cos\varphi \quad (28)$$

– The case of non-associated plasticity

$$\dot{\boldsymbol{\varepsilon}}^P = \lambda \frac{\partial g}{\partial \dot{\boldsymbol{\sigma}}} \quad \text{with} \quad g = \frac{1}{2} \left(\sigma_3 - \sigma_1 \right) + \frac{1}{2} \left(\sigma_3 + \sigma_1 \right) \sin\psi + \text{const} \quad (29)$$

Finally, the incremental stress-strain relation is derived as bellows:

$$\dot{\boldsymbol{\sigma}} = \left[\mathbf{D} - \frac{1}{d} \mathbf{a} \mathbf{b}^T \right] \dot{\boldsymbol{\varepsilon}} \quad (30)$$

According to Mohr-Coulomb yield criterion, the parameters in Eq. (30) can be deduced as:

$$\mathbf{D} = \frac{G}{1/2 - \upsilon} \begin{bmatrix} 1-\upsilon & \upsilon & \upsilon \\ \upsilon & 1-\upsilon & \upsilon \\ \upsilon & \upsilon & 1-\upsilon \end{bmatrix} \quad \text{with} \quad G = \frac{E}{2\,(1+\upsilon)} \quad (31)$$

$$d = \frac{\partial f^T}{\partial \boldsymbol{\sigma}} \mathbf{a} = G \left(1 + \frac{\sin\varphi \sin\psi}{1 - 2\upsilon} \right) \quad (32)$$

$$\mathbf{a} = \mathbf{D} \frac{\partial g}{\partial \boldsymbol{\sigma}} = \frac{G}{1-2\upsilon} \begin{bmatrix} -1 + 2\upsilon + \sin\psi \\ 2\upsilon \sin\psi \\ 1 - 2\upsilon + \sin\psi \end{bmatrix} \quad (33)$$

$$\mathbf{b}^T = \frac{\partial f^T}{\partial \boldsymbol{\sigma}} \mathbf{D} = \begin{bmatrix} -1 + 2\upsilon + \sin\varphi & 2\upsilon \sin\varphi & 1 - 2\upsilon + \sin\varphi \end{bmatrix} \quad (34)$$

3. Validation

3.1. Finite element analysis procedure

This study uses the field test results of Kim et al. [8, 10] in order to validate the results of the finite element analysis procedure. The load test site is located at the mouth of the Nakdong River in the Busan, South Korea as shown in Figure 1. The top-base foundation is placed on the sedimentary soil layer. That is soft silty sand layer. Its SPT N-value ranges from 4 to 13. The input data for FEA is given in the Table 1.

Table 1. *Input data for finite element analysis*

Grading	Unit weight	Cohesion	Friction angle	Young's modulus	Poisson's ratio
	$\gamma[kN/m^3]$	$c[kPa]$	$\varphi[^0]$	$E[kPa]$	$\nu[-]$
Top-block	23	-	-	21,000,000	0.15
Crusher-run	19	0	42	100,000	0.33
Soft sedimentary layer	17	0	25	27,000	0.35
Sedimentary layer	18	0	26	28,000	0.35

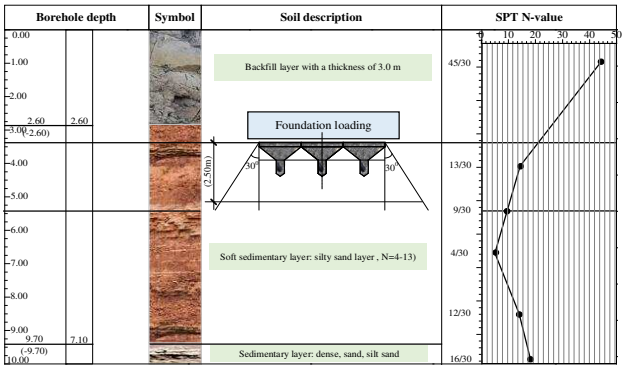

Figure 1. *Ground geology in the load test for top-base foundation*

3.1.1. Finite element model for the ground

The ground model used for FEA is a combination of pore-diffusion liquid and soil skeleton. Under the impact of the top-base foundation, the diffusion of liquid pressure interacts with the soil skeleton to create a practical stress as given in Eq. (1). Therefore, this study approaches the problem by FEA procedure, the 10-node tetrahedral element (shown in Figure 2) is used. The degrees of freedom at each node of the element are in addition to displacements in 3 directions, x, y, z (displacement field $\boldsymbol{v}$) also generate additional degrees of freedom, pore pressure $\mathbf{p}_n$ (seen in section 2.3).

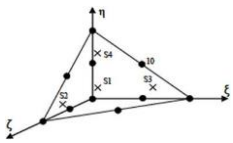

Figure 2. *The element used to generate the mesh*

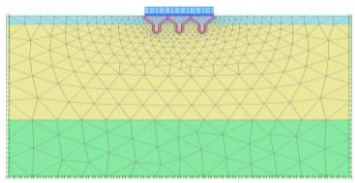

Figure 3. *The element used to generate the mesh*

The soil ground contains 3 layers: First layer is the crusher-run, and its thickness is about 0.25m; Second layer is the soft sedimentary layer, and its layer is about 3.75m; Third layer is the sedimentary layer, and its thickness is about 5.70m. The mesh generation for the soil ground is given in the Figure 3.

3.1.2. Finite element model for the top-block

TBF consists of 2 components, the crusher-run ground, and the top-block layer. In which, the crusher-run ground has completely similar properties to the natural soil ground. Therefore, the crusher-run layer is considered as a soil layer of the ground, and its FEA has just been presented in section 3.1.1. Another is a top-block layer that cast in-situ concrete. The size of a top-block to work most efficiently investigated in the study of Kim et al. [8] and is given as in Figure 4a. The interaction conditions between the top-blocks and the crusher-run layer are presented in section 2.4.

The concrete material model of the top-block block in FEA analysis uses the model in the study of Le et al, [19]. In this study, the top-blocks use the 3D-stress element C3D8R to generate the mesh. This is an 8-node brick element with the technique of reducing to a Gauss integral point, so the shear locking phenomenon is overcome, the stress-strain relationship has high accuracy. Since only one integral point is located at the centroid of the element, the computational cost is greatly reduced. At the same time, the small size elements will accurately describe the stress concentration at the corner and boundary positions of the structures. The mesh generation is shown in Figure 4b.

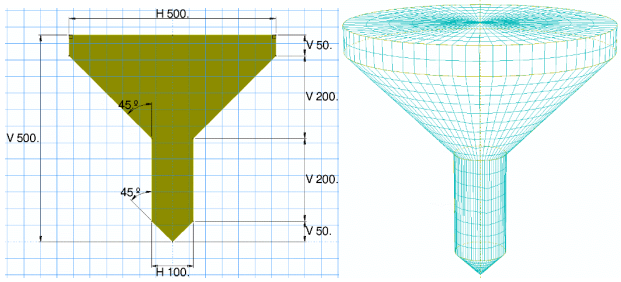

Figure 4. *a) Top-block geometry; b) Top-block mesh in FEA*

3.2. Validation

The loading process proceeds gradually, and the displacement/strain sensors were set up to determine the settlement and fracture shape when the ground is cut as in the studies of Kim et al., [8, 10]. This process was re-simulated by using the FEA, the simulation results were validated with the experimental results of Kim et al. From this validation, the accuracy and reliability of the FEA procedure are evaluated. In this study, the FEA results were compared with the experimental results of the TBF in the study of Kim et al., [8] shown in Figure 5 and Table 2.

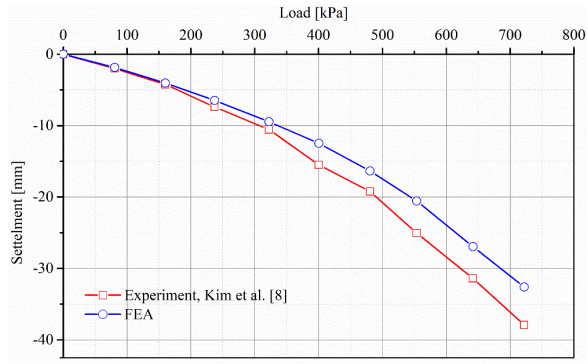

Figure 5. *Validate FEA results with field tests [8]*

Table 2. *Compare FEA results with field tests [8]*

No	P-Load	Settlement		Error
		Experiment	FEA	
	[kPa]	[mm]	[mm]	[%]
1	0	0	0	0
2	80.47	-2.01	-1.86	7.30
3	160.00	-4.23	-4.03	4.62
4	237.21	-7.39	-6.47	12.45
5	322.33	-10.55	-9.468	10.30
6	400.47	-15.50	-12.47	19.54
7	480.70	-19.23	-16.36	14.94
8	553.72	-25.04	-20.57	17.85
9	641.86	-31.40	-26.95	14.18
10	722.09	-37.93	-32.62	14.00
Average error				**11.52**

The analysis results in Figure 5 show that the tendency of settlement development in the TBF between the experiment and the FEA is resemble. The results of error assessment on each load level are given in Table 2. The

error ranges from 4.5% at 160 kPa loading level to 19.5% at 400 kPa loading level. The error increases with respect to the increase of loading level. This can be explained when the load is small, the ground works in the linear elastic limit. Most FEAs use the linear elastic materials that can precisely simulate with respect to real model. When starting from the loading level of 400 kPa, the soil begins to plasticize, and the material model of the soil is now working as an elasto-plastic model. In the FEA, the Mohr-Coulomb model is exerted (see section 2.5). This model has idealized some actual physical and mechanical properties of the ground. Hence, at the loading level of 400 kPa, the settlement of the TBF has a sudden change, while the FEA has not reflect the actual behavior at this loading level. As a result (8a), the error at this loading level is 19.5%. After passing the loading level of 400 kPa, the ground is reinforced and the bearing capacity is relatively stable. In these loading levels, the FEA results reflect relatively like the experimental results, and the error in these loading levels fluctuates around 14.5%.

The results of the evaluation error on the entire model are about 11.52%. This result shows that the FEA procedure is relatively accurate and reliable. Although soil material contains solid, liquid and gas phases with very complex behavior, and it is very difficult to predict results accurately. At force level 722 kPa, the displacement field in the TBF is shown in Figure 6. The results in Figure 6 demonstrate(9a) a reasonable displacement distribution and ensure reliability.

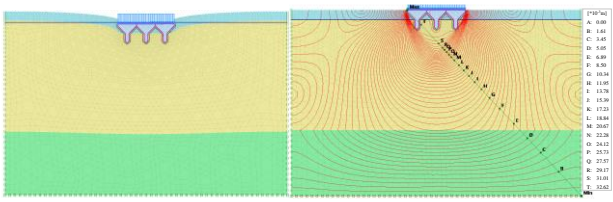

Figure 6. *The displacement field of the top-base foundation*

In addition to increase the accuracy and reliability of the FEA procedure, this study also compares the FEA results with the laboratory tests of Kim et al., [10].

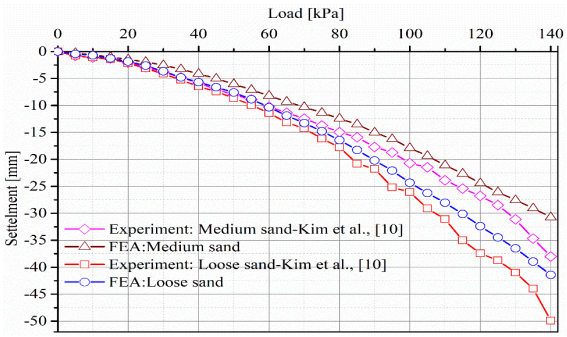

Figure 7. *Verify FEA results and lab tests [10]*

In this experiment, Kim et al., tested the TBF on two types of medium sand and loose sand. The comparison results are shown in Figure 7. The results demonstrated the similarity between the experimental model and the finite element model as in analysis. But the error in this comparison result is smaller, it ranges from (7.0-9.0) % compared to the results (seen Table 3). The reason is that it was performed in the laboratory with a model of 1/5 times smaller than the actual model, and the maximum loading level is only 140 kPa.

Thus, this claims that FEA results ensure accuracy and reliability. The FEA can be exerted to analyze and evaluate similar buildings without having to conduct experiments (or field tests) that require a lot of time-consuming and experimental expense.

4. Application

In this study, the FEA procedure is applied to evaluate the effectiveness of the TBF option in the design with respect to projects with small and medium loads.

The applied project contains 1 basement and 14 floating floors. The ground floor as well as others are symmetrically designed, the basement is used to arrange the underground water basin, the technical room, the remaining area is used for car and motor parks(5b). The first floor is used to arrange a large reception hall, administrative-material supply room, propaganda and support room, dining room, coffee area for entertainment needs. In addition, 2 more toilet blocks, 3 stairs and 1 elevator are arranged to organize vertical traffic between floors. The 2nd floor has an atrium with the 1st floor, a large meeting room and a break hall for the meeting room, an additional large office room, a small office room with an interior toilet area. The first two floors designed with a rectangular shape are larger than the typical floors, it forms a podium to support the high-rise tower (1b). The 3rd to the 12th floor is used for offices, meeting rooms, corridors, etc(2b). The 13th floor contains the following function rooms: the storage room, document editing room, elevator technical room(3b). The roof floor is arranged with roof water tank, waterproofing, heat-proof, and lightning-protection system. The load used to design the foundation for the building is shown in Table 3.

Table 3. *Load combination using foundation design*

Position	Element	Ultimate limit states					Serviceability limit states				
		M_x	M_y	N	Q_x	Q_y	M_x	M_y	N	Q_x	Q_y
		$kN.m$	$kN.m$	kN	kN	kN	$kN.m$	$kN.m$	kN	kN	kN
7-C	C38	-18.3	189.9	-5246.0	-10.5	87.9	-15.9	165.1	-4561.7	-9.1	76.4

The building placed on a soft ground has(10a) the mechanical and physical properties as shown in Table 4. With the above-mentioned construction and soil properties, in the structural design, it was proposed the of bored pile foundation for high-rise tower and pressed piles foundation for podium, and it is described in Figure 8.

Table 4. *Mechanical-physical properties of the soil ground(11a)*

Grading	Unit weight	Cohesion	Friction angle	Young's modulus	Poisson's ratio
	$\gamma[kN/m^3]$	$c[kPa]$	$\varphi[^0]$	$E[kPa]$	$\nu[-]$
Backfill soil	17.67	7.13	8.08	4854.29	0.31
Loam (soft)	17.89	9.12	7.08	5177.91	0.33
Fine sand, gray-green (loose)	18.56	0.00	26.30	8433.72	0.29
Clay, gray-green (liquid)	17.20	8.83	3.67	2745.86	0.34
Clay, brown-red (semi-dense)	19.15	24.61	16.47	16318.27	0.28

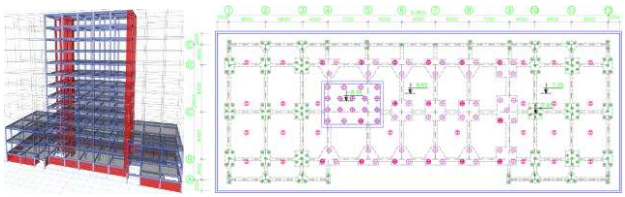

Figure 8. *Construction structure and foundation plan*

In the design, a bored pile of diameter 600mm(4b) is used, and the depth of the pile tip is 28m calculated from the natural ground. The settlement plot under the bottom of the conventional pile foundation is shown in Figure 9.

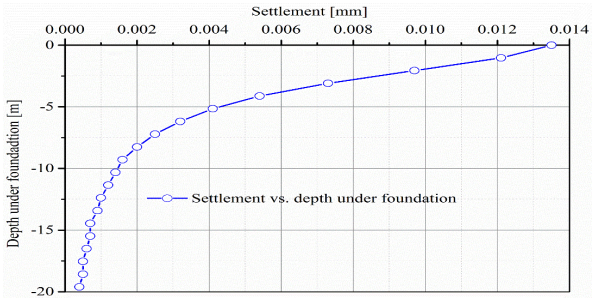

Figure 9. *Settlement of the conventional pile foundation*

According to the TCVN 9362-2012 standard, the settlement limit of the foundation is considered to the 6th settlement point at a depth of 6,192 (m) calculated from the bottom of the conventional pile foundation. The final settlement result of the pile foundation is as follows:

$$s = \sum_{i=1}^{n} \frac{\beta}{E_i} \cdot \sigma_{zi}^{gl} \cdot h_i = 5.21 \ cm \ \leq [s] = 8 \ cm \quad (35)$$

Now, in this study, we change the pile foundation option by the TBF, by using a two-way strip foundation placed on the top-base ground. Then FEA is used to analyze and evaluate the effectiveness of the TBF with respect to pile foundation.

4.1.1. Finite element model

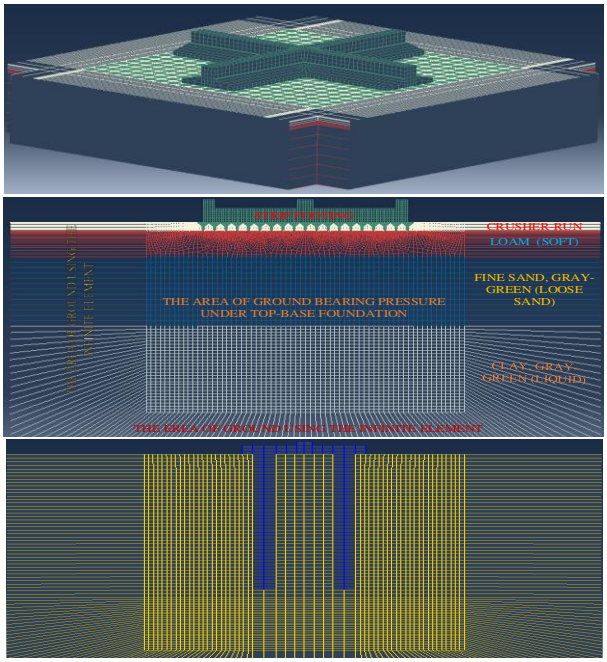

Figure 10. *FEA model of top-base and pile foundations*

TBF and pile foundation use the finite element model presented in sections 3.1.1 and 3.1.2. In this analysis, an infinite boundary element is used (the infinite element instead of boundary conditions around the soil ground in order to reduce the ground size during analysis. But it still ensures that the model works close to reality and the simulation results ensure accuracy). The finite element model of the soil ground is shown in Figure 10.

4.1.2. Analyze the results

a. Displacement

The simulation results in Figure 11 show that the 1-layer TBF reaches the maximum settlement of 1.25cm at the loading level of 11.5 MN, the 2-layer TBF reaches the maximum settlement of 0.5cm at the loading level of 25.6 MN and the pile foundation reaches the maximum settlement of 5cm at the loading level of 6.6 MN. The displacement spectrum distributed in the soil ground is shown in Figure 12.

Thus, the bearing capacity of the 1-layer TBF is 1.74 times higher than that of the pile foundation, while its settlement is only 0.2 times that of the pile foundation. Similarly, the 2-layer TBF is 3.88 times higher than the pile foundation, while its settlement is only about 0.08 times that of the pile foundation. This shows that the criterion of settlement and load-carrying capacity of the top-base foundation is superior to that of the pile foundation.

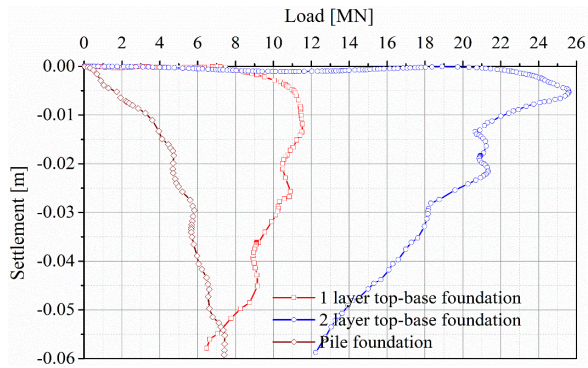

Figure 11. *Settlement analysis of the foundations by FEA*

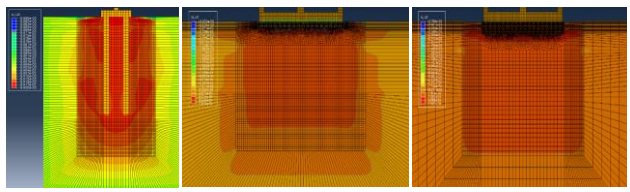

Pile foundation. *1-layer TBF.* *2-layer TBF.*

Figure 12. *Displacement spectrum distributed in the ground*

Theoretical calculation according to TCVN 9362-2012, we have the settlement of the pile foundation 5.21 cm (see Eq. (35)) at the loading level of the foundation 5.25 MN (seen Table 3). According to the results of FEA at the loading level of 5.25 MN, the settlement of the foundation is 2.82 cm (seen Figure 11). This settlement result is equal to 0.55 times the theoretical result. But according to the results of FEA analysis, the foundation still has bearing capacity and when the foundation reaches a settlement of 5.21 cm, the corresponding loading level that the foundation can withstand is 6.95 MN, and this is 1.34 times

higher than the theoretical result. This result is reasonable because in the design standard, the factor of safety is considered, which is not considered in the FEA analysis.

When increasing the quantity of top-base layer become to 2-layer TBF, the bearing capacity of the top-base foundation increased by 2.23 times and the settlement decreased by 0.4 times compared to the 1-layer TBF. This demonstrates that for projects requiring severe settlement and large bearing capacity, then the number of top-base layers can be increased.

b. Stress

Determining the stress field distributed in the ground is also one of the essential factors. Because when we know the exact stress distribution field, then stress concentration on which ground area will be specifically analyzed, and whether the allowable strength of the soil ground in those areas is guaranteed or not? Thence, it helps us to accurately predict the locations where the ground will be damaged early. Also, it helps the designer to make reasonable adjustments to the design of the foundation, that increases the load-carrying capacity of the foundation. Inversely, in the experimental model, it is difficult to determine the stress distribution field in the top-base layer and soil ground accurately, and when implementing requires a huge investment of cost, time, and effort. The establishment of the FEA procedure is extremely convenient for determining the stress distribution field in the top-base layer and the soil ground. The results of which are shown in Figure 13.

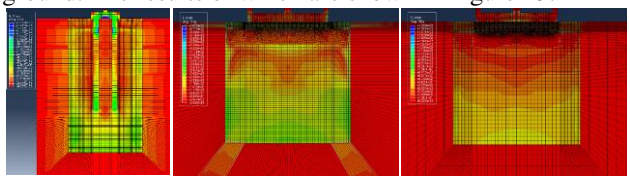

Pile foundation. *1-layer TBF.* *2-layer TBF.*

Figure 13. *Stress spectrum distributed in the ground*

The results show that the stress distribution in the TBF is quite large but the stress distribution in the soil layer under the TBF is very small. These exposures the effective promotion of the TBF, it redistributes the pressure/stress from the foundation to the ground evenly. At the same time, because the top-block structure has a conical shape, it is naturally the top-base itself absorbs the pressure of the foundation transmits to the ground. For the 2-layer TBF, the stress distribution under the top-base layer is more uniform than that of the 1-layer TBF.

5. Conclusion

The study has developed the FEA procedure for TBF problem. The analysis results claim that the FEA procedure has accurately simulated the behavior of the TBF through validation of the actual experimental results in the field and in the laboratory tests. Simultaneously, the results of applying the FEA procedure with respect to the actual building demonstrate the rationality and accuracy of the FEA procedure(12a) (6b). In addition, the results of using FEA are biased towards safety in the design problem. Therefore, in similar design problems, this FEA procedure can be exerted to reduce the cost, time, and effort for the experiment in the design problem.

REFERENCES

[1] Arai, K., H. Machihara, M. Horita, and I. Yasukawa, "Laboratory tests and analysis on settlement and bearing capacity of foundation with top-shaped concrete blocks", *The proceedings of 32nd Symposium of JSSMFE on Foundation Procedures without Piles*, 1987, 55-60.

[2] Arai, K., Y. Ohnishi, M. Horita, and I. Yasukawa, "Measurement and interpretation of loading tests of concrete top blocks on soft ground", *International symposium on field measurements in geomechanics, 2*, 1988, 1177-1184.

[3] Arai, K., I. Yasukawa, Y. Ohnishi, M. Horita, and S. Nakaya, "Interpretation of concrete top base foundation behaviour on soft ground by coupled stress flow finite element analysis", *Numerical Methods in Geomechanics Innsbruck 1988*, 2017, *Routledge*. 625-630.

[4] Yamada, K., L. Yasnkwa, and M. Saitoh, "In-Situ plate Loading Test of Concrete Top Block on soft gronnd", *The proceedings of Annual Conference of JSSMFE*, 1986, 1281-1284.

[5] Shin, E.-C. and M.-H. Ahn, "Estimation of Bearing Capacity for In-Situ Top-Base Method by Field Experimental Plate Load Test", *J. Korean Geosynthetics Society*, 2011, 10(1), 1-8.

[6] Chung, J.-H., H.-K. Chung, and S. Lee, "Behavior of floating top-base foundation on soft soils by laboratory model tests", *Journal of the Korean Geotechnical Society*, 2011, 27(2), 5-15.

[7] Kang, H.-K., C.-K. Kim, B.-Y. Lee, and H.-M. Kim, "Model Test on the Effect of Bearing Capacity for In-situ Top Base Method in sand", *Proceedings of the Korean Geotechical Society Conference*, 2005, Korean Geotechnical Society, 597-602.

[8] Kim, H.-M. and C.-K. Kim, "The Behavior of In-situ Top Base foundation in Granular Soil", *Journal of the Korean Geotechnical Society*, 2008, 24(10), 121-129.

[9] Li Guo-wei, Y.Y.-j., Xiong Li, Wu Jiang-Tao, Cao Xue-Shan, "Field tests on top-shaped concrete block cushion-reinforced soft soil foundation drained with sand bag well", *Chinese Journal of Geotechnical Engineering*, 2021, 43(3), 425-431.

[10] Kim, C.-K. and H.-M. Kim, "The Bearing Capacity Characteristics of Top Base Foundations in Cohesionless Soils", *Journal of the Korean Geotechnical Society*, 2010, 26(7), 135-145.

[11] Chung, J.-H., H.-K. Jung, and S. Lee, "Behavior of Floating Base Plate by Stress Delivery Mechanism", *Journal of the Korea institute for structural maintenance and inspection*, 2010, 14(2), 137-144.

[12] Terzaghi, K., R.B. Peck, and G. Mesri, *Soil mechanics in engineering practice*, John Wiley & Sons, 1996.

[13] Biot, M.A., "General solution of the equations of elasticity and consolidation for a porous material", *J. Appl. Mech*, 1956, 23, 91-95.

[14] De Borst, R., M.A. Crisfield, J.J. Remmers, and C.V. Verhoosel, *Nonlinear finite element analysis of solids and structures*, John Wiley & Sons, 2012.

[15] Bonet, J. and R.D. Wood, *Nonlinear continuum mechanics for finite element analysis*, Cambridge university press, 1997.

[16] Collins, R.E., *Flow of fluids through porous materials*, Petroleum Publishing Company, 1976.

[17] Song, E.-x., *Elasto-plastic consolidation under steady and cyclic loads*, Diss. Technische Universiteit Delft, 1990.

[18] Barneveld, A., *FEM based soil stress and strain analyses aimed at plant growth factors*, Wageningen University and Research, 2000.

[19] Minh, H.-L., S. Khatir, M.A. Wahab, and T. Cuong-Le, "A concrete damage plasticity model for predicting the effects of compressive high-strength concrete under static and dynamic loads", *Journal of Building Engineering*, 2021, 44, 103239.